



Molecular Crystals and Liquid Crystals Science and Technology. Section A. Molecular Crystals and Liquid Crystals

Publication details, including instructions for authors and
subscription information:

<http://www.tandfonline.com/loi/gmcl19>

Mixed-Valence States in MMX-Chains Complex, $\text{Pt}_2(\text{dta})_4\text{I}$

Hiroshi Kitagawa^a, Noriaki Onodera^a, Jeung-Sun Ahn^a,
Tadaaki Mitani^a, Misa Kim^b, Yoshiki Ozawa^b, Koshiro Toriumi^b
, Kazutomo Yasui^c, Toshio Manabe^c & Masahiro Yamashita^c

^a Japan Advanced Institute of Science and Technology,
Tatsunokuchi, Ishikawa, 923-12, Japan

^b Himeji Institute of Technology, Harima Science Park City,
Hyogo, 678-12, Japan

^c Nagoya University, Chikusa-ku, Nagoya, 464-01, Japan

Version of record first published: 24 Sep 2006.

To cite this article: Hiroshi Kitagawa, Noriaki Onodera, Jeung-Sun Ahn, Tadaaki Mitani, Misa Kim, Yoshiki Ozawa, Koshiro Toriumi, Kazutomo Yasui, Toshio Manabe & Masahiro Yamashita (1996): Mixed-Valence States in MMX-Chains Complex, $\text{Pt}_2(\text{dta})_4\text{I}$, Molecular Crystals and Liquid Crystals Science and Technology. Section A. Molecular Crystals and Liquid Crystals, 285:1, 311-316

To link to this article: <http://dx.doi.org/10.1080/10587259608030818>

PLEASE SCROLL DOWN FOR ARTICLE

Full terms and conditions of use: <http://www.tandfonline.com/page/terms-and-conditions>

This article may be used for research, teaching, and private study purposes. Any substantial or systematic reproduction, redistribution, reselling, loan, sub-licensing, systematic supply, or distribution in any form to anyone is expressly forbidden.

The publisher does not give any warranty express or implied or make any representation that the contents will be complete or accurate or up to date. The accuracy of any instructions, formulae, and drug doses should be independently verified with primary sources. The publisher shall not be liable for any loss, actions,

claims, proceedings, demand, or costs or damages whatsoever or howsoever caused arising directly or indirectly in connection with or arising out of the use of this material.

MIXED-VALENCE STATES IN MMX-CHAINS COMPLEX, $\text{Pt}_2(\text{dta})_4\text{I}$

HIROSHI KITAGAWA, NORIAKI ONODERA, JEUNG-SUN AHN,
AND TADAOKI MITANI

Japan Advanced Institute of Science and Technology, Tatsunokuchi, Ishikawa 923-12, Japan

MISA KIM, YOSHIKI OZAWA, AND KOSHIRO TORIUMI

Himeji Institute of Technology, Harima Science Park City, Hyogo 678-12, Japan

KAZUTOMO YASUI, TOSHIO MANABE, AND MASAHIRO YAMASHITA

Nagoya University, Chikusa-ku, Nagoya 464-01, Japan

Abstract Physical and structural properties of the MMX-type halogen-bridged mixed-valence complex, $\text{Pt}_2(\text{dta})_4\text{I}$ ($\text{dta} = \text{CH}_3\text{CS}_2^-$) were investigated. This complex exhibits metallic conduction above room temperature, which is the first observation in halogen-bridged 1-D transition-metal complexes. Below 300 K, the metal-semiconductor transition was observed. The mixed-valence state of this compound is discussed.

INTRODUCTION

These twenty years halogen-bridged 1-D transition-metal complexes (MX chains) analogous to Wolfram's Red Salt have been investigated intensively from viewpoints of physics and chemistry as a model of 1-D electrons system.¹⁻³ MX chains can be regarded as a presumed 1-D metal in which the conduction band of half filling is made up primarily of an antibonding combination of the transition metal $M d_z^2$ orbitals and bridging halogen $X p_z$ orbitals. In reality, MX chains with $M=\text{Ni}$ are Mott-type or charge-transfer-type insulators due to the strong electron correlation, while MX chains with $M=\text{Pd}$, Pt are mixed-valence-type insulators in which lattice distortions of $\cdots X-M^{\text{II}}-X \cdots M^{\text{IV}} \cdots$ occur and open a gap at the Fermi energy due to the strong electron-lattice interaction. The metallization has been expected to be realized by the application of pressure. Though the extensive work on MX chains under high pressure, the insulator-to-metal transition has not been observed yet.⁴⁻⁷

In this work, we have focused on MMX system of the title complex in which there exist 1-D $\cdots \text{I}-\text{Pt}-\text{Pt}-\text{I} \cdots$ neutral chains.⁸⁻¹² The formal oxidation state of Pt in this system is +2.5, which differs from that (+3) of MX system. Another different feature is that electronic structure of the presumed 1-D half-filled conduction band is composed primarily of an antibonding combination of antibonding $M(d_z^2)-M(d_z^2)$ orbitals and $X p_z$ orbitals. Because of a direct overlapping between the M-M orbitals, the band-width of conduction band in MMX chains is expected to be wider than that in MX chains. In order to reveal the mixed-valence state and the electrical conduction in this MMX system, we have measured XPS, electrical conductivity, other physical properties of $\text{Pt}_2(\text{dta})_4\text{I}$.

EXPERIMENTAL

The title complex was prepared by the method previously reported.⁸ The single crystals were grown by slow recrystallization from toluene solutions. The quality of obtained single crystals were confirmed by X-ray single-crystal analysis, elemental analysis, and IR spectroscopy.

The *dc* electrical-conductivity measurements were performed on several single crystals with a conventional four-probe method using gold paint and gold wire (20 $\mu\text{m}\phi$).

The X-ray photoelectron spectra were obtained on a VG ESCA MKII electron spectrometer, the source vacuum being $< 1 \times 10^{-8}$ mbar, with a Mg-K α X-ray source (1253.6 eV) in the temperature range of 150 - 300 K. The pass-energy of a hemisphere analyzer was constant (20 eV). Binding energies were measured relative to the C 1s peak due to hydrocarbon contamination from the diffusion pump, which built up slowly on the surface under these operating conditions. The absolute binding energy (284.4 eV) of the contaminant C 1s peak was confirmed by measuring its energy on the surface of silver foil (Ag 3d_{5/2} = 367.9 eV) after the Ar⁺ ion sputtering to the foil. Absence of X-ray beam effects was checked by the X-ray power dependency of XPS spectra.

For optical absorption spectra, powdered samples ground down from single crystals were diluted with KBr and then the mixtures were processed into pellets under pressure (~ 6 Kbar) and vacuous condition. The UV-VIS-NIR absorption spectra were measured in the temperature range 1.4 - 450 K by a Jasco V-570 spectrometer with an OXFORD Optistat^{CF} cryostat. The infra-red (IR) absorption spectra were measured in the temperature region of 10 - 450 K by a Nicolet FTIR 800 spectrometer with a DAIKIN CryoKelvin 202CL cryostat that has KRS-5 optical windows. IR detectors of TGS and MCT were used.

Polarized reflection measurements of single crystals were made at room temperature (r.t.) in the energy range 0.1 - 4.0 eV with a microscopic system of our own making.

Polarized Raman spectra of single crystals were recorded in the temperature range of 300 - 450 K with a Jasco NR-1800 zero-dispersive triple (filter single) monochromator using a microscope. A Laser Ionics 1400-10A laser provided the exciting line (514.5 nm). Detection of the scattered radiation was by a cooled Photometrics CC200 CCD camera system. Laser power at the crystals was held to < 10 mW.

The magnetic susceptibility measurement of a polycrystalline sample was performed in the temperature range of 4 - 400 K on a Quantum Design MPMS-5 SQUID magnetometer. Because of estimative error for the total diamagnetic contributions calculated using Pascal's tables and for the subtraction of a small amount of paramagnetic impurities, such corrections were not made to the measured data.

X-ray single-crystal analysis was performed in the temperature range of 115 - 375 K on an Enraf-Nonius CAD4 diffractometer equipped with graphite-crystal monochromatized Mo-

$\text{K}\alpha$ radiation ($\lambda = 0.71073 \text{ \AA}$, 50 kV-30 mA) and a liquid N_2 gas-flow-type cryostat. The high-temperature X-ray crystal structure analysis was made in the temperature range of 275 - 465 K on a Rigaku AFC-5 diffractometer with Mo- $\text{K}\alpha$ radiation and a high-temperature apparatus. The cell dimensions have been determined and refined by the least-squares method.

RESULTS AND DISCUSSIONS

Figure 1 shows the temperature dependence of the electrical resistivity of single crystal $\text{Pt}_2(\text{dta})_4\text{I}$ parallel to the chain axis (*b*). The room-temperature conductivity is much higher ($\sigma_{r.t.} \sim 13 \text{ S}\cdot\text{cm}^{-1}$) as compared with MX and other MMX chains compounds. This compound exhibits metallic conducting above 300 K, which is the first observation in halogen-bridged 1-D transition-metal complexes. Bellitto, *et al.*⁸ and Yamashita, *et al.*¹¹ reported that this salt was not a metal but a semiconductor, which are not consistent with our recent result. This disagreement is considered to be due to the difference of experimental methods. They measured the conductivity by using compressed polycrystalline samples with a four-probe method or single crystals with a two-probe one. Below 300 K, this compound shows a metal-semiconductor transition and then the resistivity increases slowly with temperature down to 150 K. However, as can be seen in Figure 2, the behavior of the conduction below 300 K is not simple activation type. Above 300 K, anomalous behavior with negative large hysteresis was observed for the resistivity. In figure 1, the lines of 1 and 2 show the heating process up to 350 K and the cooling one down to 300 K from 350 K, respectively. In general, the resistivity curve of cooling process exists above the curve of heating one. These conductivity behaviors are expected to be related closely to valence fluctuation or valence transformation of Pt. It should be noted that Whangbo and Canadell have performed band calculations using extended Hückel methods for $\text{Pt}_2(\text{dta})_4\text{I}$.¹² They have discussed the results on the bases of a possible Peierls instability of a

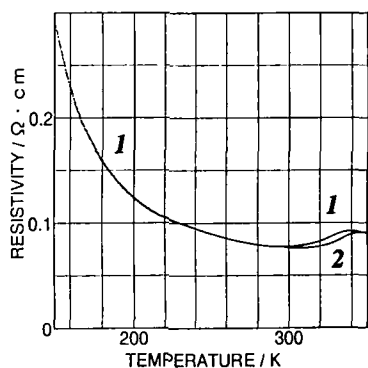


Fig. 1. Temperature dependence of the electrical resistivity of $\text{Pt}_2(\text{dta})_4\text{I}$ parallel to the chain axis (*b*).

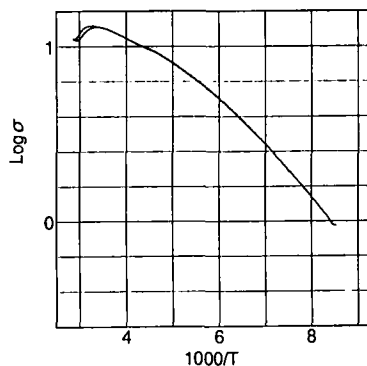


Fig. 2. Temperature dependence of the electrical conductivity of $\text{Pt}_2(\text{dta})_4\text{I}$ parallel to the chain axis (*b*).

metallic system and localized electronic states of an insulating system. The structural mode of $\text{Pt}^{2.5+}\text{Pt}^{2.5+}\text{I}-\text{Pt}^{2.5+}\text{Pt}^{2.5+}\text{I}-\text{Pt}^{2.5+}\text{Pt}^{2.5+}\text{I}-$ has been predicted to be less stable than that of $\text{Pt}^{2+}\text{Pt}^{2+}\text{I}-\text{Pt}^{3+}\text{Pt}^{3+}\text{I}-\text{Pt}^{2+}\text{Pt}^{2+}\text{I}-$, which is inconsistent with our results of X-ray single-crystal analyses mentioned below.

In order to reveal the origin of these behaviors, we measured the temperature dependence of XPS spectrum. Figure 3 shows the XPS spectra of Pt 4f region at r.t. for $\text{Pt}_2(\text{dta})_4\text{I}$ and the Pt(II) control complex, $\text{Pt}(\text{H}_2\text{DAG})_2\text{Cl}_2$ (H_2DAG = diaminoglyoxime). As can be seen in Figure 3b, the doublet is much broader having FWHMs of 1.92 eV and 2.75 eV for $4f_{7/2}$ and $4f_{5/2}$, respectively, compared with the spectrum (Figure 3c) of Pt(II) control complex (1.50 eV and 1.56 eV, respectively). So the observed spectrum was reasonably resolved into signals for Pt^{II} and Pt^{III} by using a peak-decomposition software. The binding energies of the doublet decomposed in higher energy side are typical ones for Pt^{III} compounds. The intensity of the Pt^{III} signal is smaller than that of Pt^{II} one, probably due to the partial decomposition (Pt^{III} is partially reduced to Pt^{II}) caused by the X-ray beam though careful to measure, as often observed for the halogen-bridged mixed-valence metal complexes.¹³ As previously reported by Bellitto, *et al.*, XPS spectra of Pt in $\text{Pt}_2(\text{dta})_4\text{I}$ at r.t. showed an averaged-valence state of +2.5, which is in disagreement with our recent result. One of the reasons for this discordance may be attributable to the resolution of XPS spectrometer. Most of the FWHMs observed for Pt single-valence complexes in our XPS system are ~ 1.5 eV, while ~ 2.0 eV observed for ones in their system. The spectrum at 150 K was very similar to that at r.t. It can be concluded that $\text{Pt}_2(\text{dta})_4\text{I}$ exhibits mixed valency of Pt^{II} and Pt^{III} in the temperature range 150 - 300 K. The valence fluctuation or valence transformation of Pt was not observed in the time scale of XPS ($< 10^{-16}$ sec.). In order to investigate the valence fluctuation of Pt in $\text{Pt}_2(\text{dta})_4\text{I}$, other measurements having rather longer time scales are indispensable.

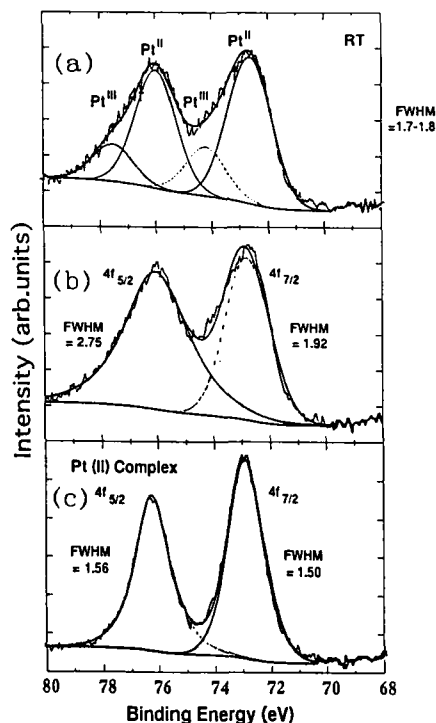


Fig. 3. XPS spectra of Pt 4f region at r.t. for (a), (b) $\text{Pt}_2(\text{dta})_4\text{I}$ and (c) $\text{Pt}(\text{H}_2\text{DAG})_2\text{Cl}_2$.

In order to make the electrical conduction clearer, the polarized reflectance spectra of the single crystal $\text{Pt}_2(\text{dta})_4\text{I}$ were measured at r.t., as shown in Figure 4. No prominent structure was observed for the polarization perpendicular to the chain axis ($E \perp b$) in the energy region from 0.1 to 4.0 eV. On the other hand, for the polarization parallel to the chain axis ($E \parallel b$), Drude-like reflectance associated with inter-binuclear charge transfer was observed, which is consistent with the metallic transport of electrons along the 1-D axis mentioned above. This anisotropic metal-like reflection shows that $\text{Pt}_2(\text{dta})_4\text{I}$ has a 1-D electronic structure. Temperature dependence of the reflectance, far-IR reflectance, and Drude analysis are in progress.

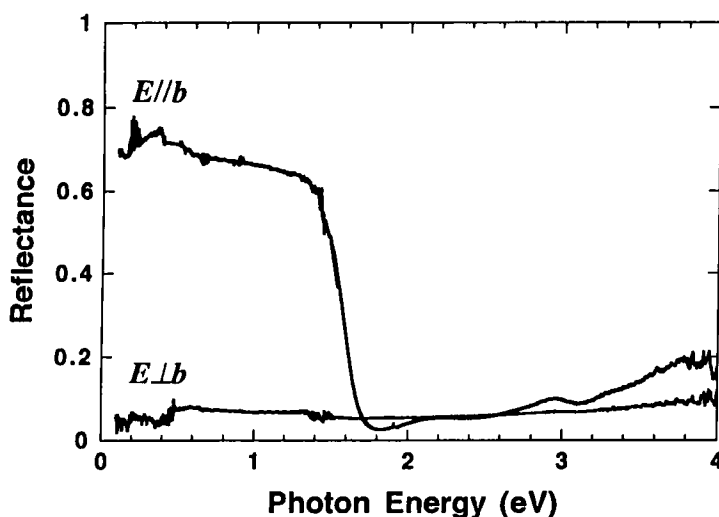


Fig. 4. Polarized reflectance spectra of the single crystal $\text{Pt}_2(\text{dta})_4\text{I}$ at r.t. for the polarization parallel and perpendicular to the chain axis (b).

Raman spectroscopy has been used widely to study the vibrational and structural properties of MX or MMX chains compounds.³ The Pt-I stretching mode was observed at 160 cm^{-1} for the polarization of parallel to the chain axis ($E_i \parallel b$). Its wavenumber is less than each of $[\text{Pt}_2(\text{pop})_4\text{I}_2]^{4-}$ (189 cm^{-1}) and $[\text{Pt}_2(\text{pop})_4\text{I}]^{4-}$ (185 cm^{-1}).¹⁴ No overtones of the Pt-I stretching mode were detected, implying a symmetric iodine bridge in this complex. The Pt-S stretching mode was also observed at 445 cm^{-1} ($E_i \perp b$). The Raman spectra of $\text{Pt}_2(\text{dta})_4\text{I}$ do not change significantly on going from 300 to 450 K.

In order to clarify the origin of the metal-semiconductor transition observed at 300 K, the temperature dependence of magnetic susceptibility was measured. The magnetic susceptibility of $\text{Pt}_2(\text{dta})_4\text{I}$ increases slightly upon cooling down to 50 K ($\chi_{r.l.} = -3.0 \times 10^{-5}$ (emu/mol) and increases rapidly to 4.2 K that is due to a small amount of paramagnetic impurities. If the transition relates to Peierls (CDW) or Spin-Peierls instability, the (spin) susceptibility should be activated below the transition. No anomaly in the susceptibility was observed at 300 K. ESR measurement may provide a better characterization of the electronic properties of this system; bandwidth, role of electron-electron interaction, and nature of the ground state, which is indispensable and in progress.

The lattice parameters were found to exhibit an anomalous temperature dependence with a negative hysteresis for the cell volume in the temperature range of 255 - 375 K. From single-crystal X-ray structure analyses at the temperatures below the transition (184 K) and above it (403 K), it was revealed that the first-order phase transition occurs from the low-temperature phase with space group $C2/c$ to high-temperature phase of $A2/m$ of which the cell volume is half the low-temperature one. In fact, this complex shows an endothermic peak in the differential-scanning-analysis (DSC) curve near 370 K on heating. The $\text{Pt}_2(\text{dta})_4\text{I}$ complex has a helical arrangement of the four dta-ligand planes around the central Pt-Pt axis. This helical structure of Pt dimer was found to be ordered in the low-temperature phase, while disordered in the high-temperature phase. It has been unknown whether the metal-insulator transition at 300 K is correlated with this order-disorder transition or not. At the present study, the bridging I atom in each phase was determined to be ordered at the midpoint of two Pt dimers. Final X-ray structural analyses are in progress.

REFERENCES

1. H. J. Keller, in Extended Linear Chain Compounds, edited by J. S. Miller, (Plenum, New York, 1982), Vol. I, p.357.
2. P. Day, in Low-Dimensional Cooperative Phenomena, edited by H. J. Keller, (Plenum, New York, 1974), p.191.
3. R. J. H. Clark, in Mixed Valence Compounds, edited by D. E. Brown, (Reidel, Dordrecht, 1982), p.271.
4. L. V. Interrante, K. W. Browall, and F. P. Bundy, Inorg. Chem., **13**, 1158 (1974).
5. L. V. Interrante and F. P. Bundy, J. Inorg. Nucl. Chem., **39**, 1333 (1977).
6. I. Shirotni, A. Kawamura, M. Yamashita, K. Toriumi, H. Kawamura, and T. Yagi, Synthetic Metals, **64**, 265 (1994).
7. H. Okamoto, private communication.
8. C. Bellitto, A. Flamini, L. Gastaldi, and L. Scaramuzza, Inorg. Chem., **22**, 444 (1983).
9. R. J. H. Clark and J. R. Walton, Inorg. Chem. Acta, **129**, 163 (1987).
10. S. Kinoshita, H. Wakita, M. Yamashita, J. Chem. Soc., Dalton Trans., 2457 (1989).
11. M. Yamashita, Y. Wada, K. Toriumi, and T. Mitani, Mol. Cryst. Liq. Cryst., **216**, 207 (1992).
12. M.-H. Whangbo and E. Canadell, Inorg. Chem., **25**, 1727 (1986).
13. M. Yamashita, I. Murase, and I. Ikemoto, Bull. Chem. Soc. Jpn., **58**, 2697 (1985).
14. M. Kurmoo and R. J. H. Clark, Inorg. Chem., **24**, 4420 (1985).